

Influence of Ni Promotion on Liquid Hydrocarbon Fuel Production over Co/CNT Catalysts

Shurong Wang,* Qianqian Yin, Jinfeng Guo, and Lingjun Zhu

State Key Laboratory of Clean Energy Utilization, Zhejiang University, Hangzhou 310027, China

ABSTRACT: An experimental study of the improved Fischer–Tropsch synthesis was conducted over a series of Ni-promoted Co/CNT catalysts to investigate the influence of Ni content on the synthesis of liquid hydrocarbon fuel (C_5 – C_{20}). The catalysts were prepared using the impregnation method and were systematically characterized by N_2 physisorption studies, X-ray diffraction, transmission electron microscopy, and hydrogen temperature-programmed reduction. The Ni promoter played a significant role in product distribution. The long-chain hydrocarbons were effectively hydrocracked because of the activity of Ni in C–C bond cleavage. A proper degree of Ni promotion could maximize the production of liquid hydrocarbon fuel. The highest selectivity for liquid hydrocarbon fuel (61.6%) and a CO conversion of 92% were obtained over the 20 wt % Co/CNT catalyst promoted by 0.5 wt % Ni.

1. INTRODUCTION

Fischer–Tropsch synthesis (FTS) is an attractive route for producing high-quality liquid fuels from alternative sources of petroleum, such as coal, natural gas, and biomass. The renewed interest in FTS has been caused by the limited supply of crude oil reserves and the excellent quality of synthetic liquid fuels. Moreover, recent improvements in gas-to-liquid technology have made these processes more efficient and cost-competitive.

The most investigated and archetypal catalysts for FTS are Fe- and Co-based materials.¹ The supports used in FTS include Al_2O_3 , SiO_2 , TiO_2 , and MgO . However, a drawback of these support materials is their reactivity toward Co, which leads to the formation of mixed compounds such as Co_2SiO_4 , Co_2AlO_4 , and $CoTiO_4$; such compounds can be reduced at high temperatures only.² Therefore, the use of carbon supports to avoid these problems has attracted a growing amount of interest.^{3–7} Carbon nanotubes (CNTs) used as support media for heterogeneous catalysis have interesting properties, such as high mechanical strength and a mesoporous structure.⁴ In addition, CNT supports can be easily removed from the catalysts by oxidation to recover precious metals.² Thus, CNTs have attracted a growing amount of attention because of their use as catalyst supports in the FTS process. Zaman et al.⁵ presented a C_{5+} selectivity of 49.9% and a CO conversion of 10.6% over a Co-based CNT catalyst. Zhang et al.⁶ found that the Pt- and Ru-promoted Co/CNT catalysts exhibited CO conversions of 37.1 and 31.4%, respectively, while the selectivities of both for C_{5+} hydrocarbon reached 80%.

The conventional FTS product distribution obeys the Anderson–Schulz–Flory statistical model; this distribution poses a limit to the maximal level of production of liquid fuel. In addition, conventional FTS is likely to yield heavier hydrocarbons (C_{21+}), which require subsequent processes for obtaining the liquid hydrocarbons (C_5 – C_{20}). This further requirement increases the cost and complexity of fuel production.^{8,9}

Ni-based catalysts have been proven to have excellent activity in the hydrocracking of hydrocarbons and significant selectivity for internal C–C bond cleavage.^{10–13} Haan et al.¹³ found that

in the hydrocracking of FTS wax over 4.5% Ni catalyst, a diesel selectivity of 74.9% was obtained at a conversion of 51.6%. These findings demonstrate that long-chain FTS products could be hydrocracked in situ over Ni-promoted FTS catalysts. In general, gasoline distillate is composed of hydrocarbons with a carbon number of 5–12, whereas hydrocarbons with a carbon number of 10–20 can be found in diesel distillate.^{14–16} In this work, liquid hydrocarbon fuel is defined as the mixture of hydrocarbons with a carbon number of 5–20. Therefore, this work was undertaken with the aim of studying the effect of Ni promotion on the direct synthesis of liquid hydrocarbon fuel over Co/CNT catalysts.

2. EXPERIMENTAL SECTION

2.1. Catalyst Preparation. Raw CNT supports were refluxed in a 30 wt % HNO_3 solution for 6 h at 373 K in a flask. The acid treatment before the preparation of the catalysts can introduce oxygenated functional groups that will increase the hydrophilicity of the CNTs and make the surface more accessible to the aqueous solution of the metal precursor.^{5,7} The mixture was filtered and washed with distilled water until the washing pH reached 7 and then dried at 363 K overnight. For the preparation of the CNT-supported catalysts, an ultrasound-assisted impregnation method was developed. Three grams of CNTs was added to a 20 mL aqueous solution of $Co(NO_3)_2$ at a concentration of 0.66 mol/L. The suspension was treated under ultrasonic conditions for 40 min and then stirred for an additional 5 h at ambient temperature. Subsequently, the Co/CNT catalyst was filtered and dried at 363 K overnight. Ni-promoted catalysts were prepared by adding 3 g of Co/CNT to 20 mL aqueous solutions of $Ni(NO_3)_2$ at concentrations of 0.01, 0.04, and 0.10 mol/L while the solutions were being stirred. The resulting catalyst samples, denoted Co/CNT, 0.5Ni-Co/CNT, 2.0Ni-Co/CNT, and 5.0Ni-Co/CNT, had 0, 0.5, 2.0, and 5.0 wt % Ni content, respectively, and a Co loading of 20 wt %. All samples were dried at 363 K and then calcined at 773 K for 5 h under a nitrogen atmosphere.

2.2. Catalyst Characterization. The Brunauer–Emmett–Teller (BET) surface areas, pore volumes, and pore size distributions of the

Received: April 23, 2013

Revised: June 20, 2013

Published: June 20, 2013



prepared catalysts were determined from nitrogen adsorption–desorption isotherms obtained at 77 K using a Quantachrome Quadasorb SI apparatus. Before the measurement, each sample was degassed at 573 K for 3 h. The specific surface area was calculated on the basis of the multipoint BET method. Powder X-ray diffraction (XRD) analysis of the catalysts was conducted on a PANalytical X'Pert PRO X-ray diffractometer with a Cu $\text{K}\alpha$ radiation source operating at 40 kV and 30 mA. The particle distribution was determined by transmission electron microscopy (TEM, Philips-FEI, Tecnai G²F30). Temperature-programmed reduction of hydrogen ($\text{H}_2\text{-TPR}$) was conducted on a Micromeritics AutoChem II 2920 instrument. The catalysts were pretreated with Ar at 473 K for 60 min. After the sample had cooled to 323 K in Ar, the gas was switched to 10 vol % H_2/Ar and the catalyst was heated to 1173 K at a ramp rate of 10 K/min. The amount of H_2 consumed was monitored with a thermal conductivity detector (TCD).

The degree of reduction could be determined by the reoxidation of the reduced catalysts.^{17,18} We conducted the reduction degree measurement on a Micromeritics AutoChem II 2920 instrument. The catalysts were reduced at 723 K for 5 h and then cooled to 373 K under hydrogen. Afterward, the hydrogen was replaced with helium, which was allowed to flow for 30 min. The temperature was subsequently increased to 723 at a rate of 10 K/min. The samples were then reoxidized by pulses of 10% oxygen in helium to determine the extent of reduction; here, it was assumed that Co^0 was oxidized to Co_3O_4 .

2.3. Test of Catalytic Activity. The FTS reactions were conducted in a continuous-flow fixed-bed reactor. In each experiment, catalysts were sieved to 40–60 mesh. Three milliliters of catalyst (~1.6 g) was sandwiched in quartz sand and then was packed into a steel tube reactor with an inner diameter of 8 mm. The catalyst bed height was ~60 mm.

Before the reaction, the catalyst was activated with pure H_2 at 723 K for 5 h at a ramping rate of 3 K/min and then cooled to the reaction temperature. The flow rate of the feed syngas was controlled with a precise mass flowmeter (Brooks, 5850E). The reaction pressure was regulated with a back pressure valve (Tescom) using the feeding gas at a flow rate of 60 mL/min. The reaction temperature was monitored with a K-type thermocouple inserted into the center of the catalyst bed. The reaction temperature was controlled automatically with an electric heating system with a temperature feedback unit. The reaction is exothermic. However, the heat released during the reaction was slightly due to the small amount of catalyst loaded, and the reaction heat could be taken away effectively by high-flux gas flow. Therefore, the catalyst bed temperature could be kept constant.

The effluent stream was condensed by a trap to obtain the long-chain hydrocarbons (C_{5+}). Uncondensed effluent gas products (H_2 , CO, CO_2 , and $\text{C}_1\text{--C}_4$ hydrocarbons) were analyzed using an online gas chromatograph (GC) (Agilent 6820) equipped with a valve sampling system. H_2 , CO, and CO_2 were separated by a TDX-01 packed column (0.5 m) and then detected by a TCD, while the gaseous hydrocarbons ($\text{C}_1\text{--C}_4$) were separated by a Propack-Q packed column (1 m) and then detected by a flame ionization detector (FID). Argon was used as the carrier gas at a flow rate of 30 mL/min for the two packed columns, and the oven temperature increased from 313 to 393 K at a ramp rate of 5 K/min and then was maintained at 393 K for 30 min. The liquid products, including the oil phase and aqueous phase, were collected together every 12 h, and then the two phases were manually separated with a separatory funnel. The oil phase was analyzed quantitatively using an off-line GC (Agilent 7890A) equipped with a FID and an INNOWAX capillary column (30 m \times 0.32 mm \times 0.25 μm). Helium was used as the carrier gas at a flow rate of 2 mL/min, and the oven temperature increased from 313 to 473 K at a ramp rate of 10 K/min and then was maintained at 473 K for 15 min. In addition, the components of the oil phase were analyzed qualitatively using a gas chromatograph–mass spectrometer (GC–MS) (Thermo Scientific, Trace DSQ II) with a DB-WAX capillary column (30 m \times 0.25 mm \times 0.25 μm) using helium as the carrier gas at a flow rate of 2 mL/min. The catalytic activity tests were conducted at 1–3 MPa, a H_2/CO mole ratio of 1–4, and a gas hourly space

velocity [GHSV, the volume of syngas (STP) per volume of catalyst per hour] of 600–2400 h^{-1} .

The CO conversion and hydrocarbon selectivity were calculated on the basis of the number of moles of C, according to the following (the carbon balance was held at 100 \pm 5%)

$$X_{\text{CO}} (\%) = (n_{\text{co}_{\text{in}}} - n_{\text{co}_{\text{out}}}) / n_{\text{co}_{\text{in}}} \times 100\%$$

$$S_{\text{c}_m} (\%) = m \times n_{\text{c}_m} / (n_{\text{co}_{\text{in}}} - n_{\text{co}_{\text{out}}}) \times 100\%$$

where X_{CO} and S_{c_m} refer to the CO conversion and product selectivity, respectively, $n_{\text{co}_{\text{in}}}$ and $n_{\text{co}_{\text{out}}}$ represent the number of moles of CO in the feed and vent gas, respectively, m represents the carbon number of the product C_m , and n_{c_m} refers to the number of moles of C_m .

The blank experiments with CNT and Ni/CNT (20 wt % Ni loaded) were preliminarily conducted under the following conditions: 533 K, 2 MPa, H_2/CO mole ratio of 2, and GHSV of 1200 h^{-1} . The conversions of CO over the CNT and Ni/CNT catalysts were 0 and <1%, respectively.

3. RESULTS AND DISCUSSION

3.1. Characterization of Catalysts. Nitrogen adsorption–desorption measurements were used to evaluate the textural properties of the samples (Table 1). The BET surface area of

Table 1. Texture Properties of the Prepared Catalysts

catalyst	S_{BET} (m^2/g)	V_{pore} (cm^3/g)	D_{pore} (nm)
CNTs	449	0.642	5.7
Co/CNT	349	0.445	5.1
0.5Ni-Co/CNT	354	0.452	5.1
2.0Ni-Co/CNT	354	0.416	4.7
5.0Ni-Co/CNT	344	0.547	6.4

the supported catalysts decreased by 21.0–24.0% compared with that of the fresh CNTs, and the pore volumes of the supported catalysts decreased correspondingly, because of the introduction of the active components. In the case presented here, the dilution effect caused by the active components during the catalyst preparation was responsible for the decrease in the BET surface area, as the impregnation led to a decrease in the support concentration.^{19,20}

The pore size of the prepared catalysts followed bimodal distributions (Figure 1). The first pore size distributions for all the samples centered at 3.8 nm. The larger pore size

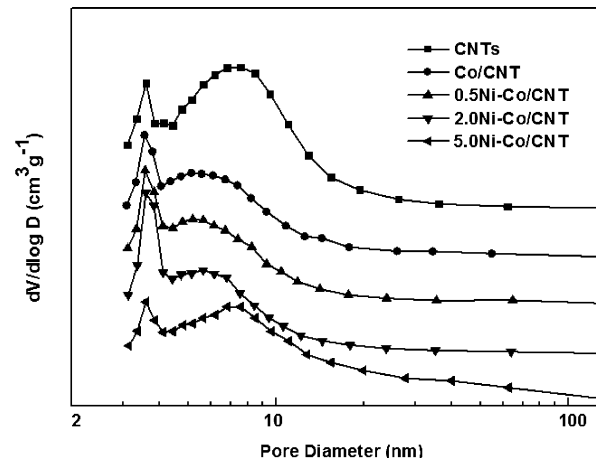


Figure 1. Pore size distributions of CNTs and the prepared catalysts.

distributions are located at 5.5 nm (Co/CNT, 0.5Ni-Co/CNT, and 2.0Ni-Co/CNT) and 7.5 nm (CNTs and 5.0Ni-Co/CNT). As shown in Table 1, the 5.0Ni-Co/CNT catalyst had a larger average pore diameter and pore volume than the 2.0Ni-Co/CNT catalyst, which might be caused by the relatively larger mesopores generated during the impregnation of a larger amount of Ni.

Figure 2 shows the XRD patterns of the fresh CNTs and CNT-supported catalysts before and after reduction, as well as

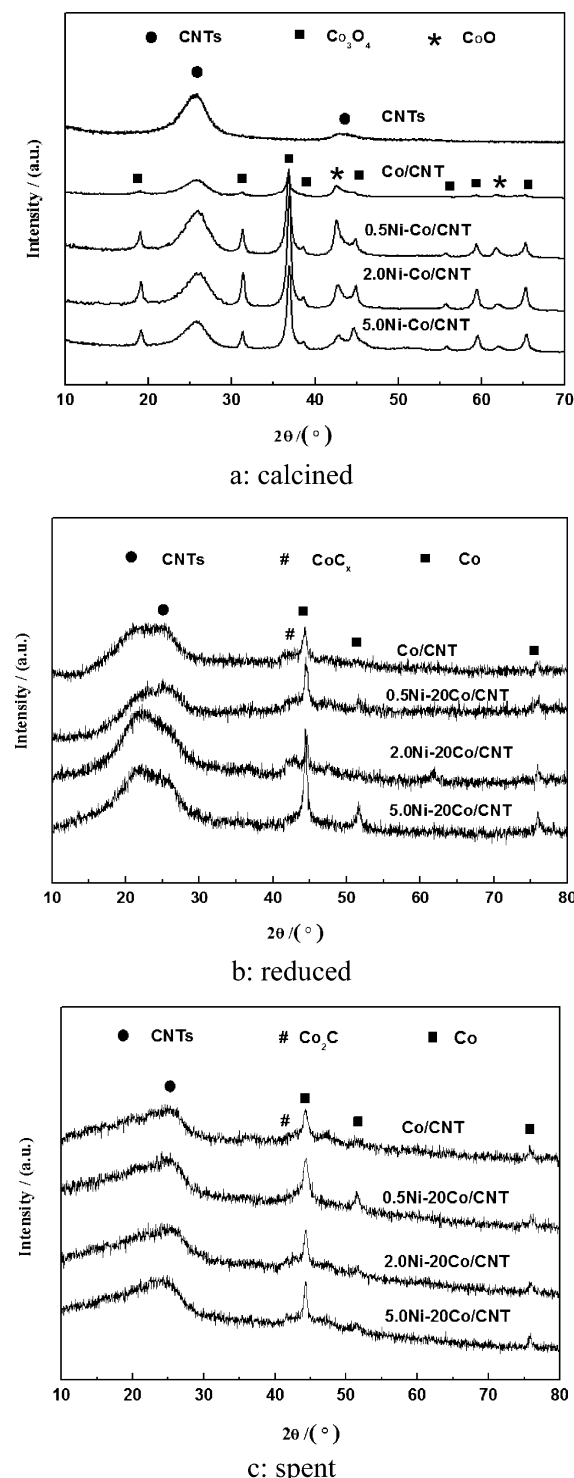


Figure 2. XRD patterns of the CNTs and different catalysts.

that of the spent catalysts. The strongest diffraction peak at 26.3° and the peak with medium intensity at 42.2° for the CNTs could be unambiguously ascribed to the (002) and (100) reflections of graphite, respectively.⁶ The XRD patterns for all calcinated catalysts show diffraction peaks at 19.0° , 31.3° , 36.8° , 38° , 44.8° , 56° , 59.4° , and 65.2° , which correspond to the various crystal planes of the Co_3O_4 phase. The CoO peaks appearing at 42.7° and 61.9° may be attributed to the autoreduction of Co_3O_4 to CoO by CNTs.²¹ It was reported in the literature that Ni and Co tend to form NiCo_2O_4 during calcination.²² Therefore, it was hard to avoid the formation of NiCo_2O_4 on Ni-Co/CNT catalysts, although no corresponding diffraction peaks were detected in the XRD patterns, mostly because of their small particle size. The average crystallite size of Co_3O_4 was calculated according to the Scherrer equation by using the diffraction lines at $2\theta = 36.8^\circ$. The crystallite sizes of Co_3O_4 increased with an increasing amount of Ni promoter: sizes of 12.0, 14.0, 15.0, and 17.0 nm for Co/CNT, 0.5Ni-Co/CNT, 2.0Ni-Co/CNT, and 5.0Ni-Co/CNT, respectively (Table 2).

Table 2. Physicochemical Properties of the Catalysts

catalyst	Co^0 (nm)					Co^0 active sites ($\mu\text{mol/g}$) ^e
	Co_3O_4 (nm) ^a	XRD ^b	TEM	red. (%) ^c	D (%) ^d	
Co/CNT	12.0	9.0	10.8	51.3	10.7	186
0.5Ni-Co/CNT	14.0	10.5	13.3	74.0	9.1	229
2.0Ni-Co/CNT	15.0	11.3	14.5	61.0	8.5	176
5.0Ni-Co/CNT	17.0	12.8	17.8	40.6	7.5	103

^aDetermined by XRD. ^bDetermined by $d(\text{Co}^0) = 0.75 \times d(\text{Co}_3\text{O}_4)$.

^cReduction degree determined by the reoxidation of the reduced catalyst. ^dDispersion was calculated by $D = 96/d(\text{Co}^0)$ (%). ^eValues derived from the reduction degree and dispersion.

The XRD patterns for the Co/CNT and the Ni-promoted catalysts after reduction are almost identical (Figure 2b). Metallic cobalt was the main phase in cobalt-based catalysts; other phases consist of graphite, as evidenced by its diffraction peaks. The diffraction peaks at $2\theta = 44.7^\circ$, 51.5° , and 75.9° are indicative of $\text{Co}(111)$, $\text{Co}(200)$, and $\text{Co}(220)$, respectively.^{23,24} The diffraction peaks at $2\theta = 42.5^\circ$ correspond to CoC_x , which is attributed to the autoreduction of cobalt species by CNTs.^{21,25} No diffraction lines originating from Ni are visible because of the small crystallite sizes of Ni.

The morphologies of Co/CNT catalysts and Ni-promoted cobalt catalysts before and after reaction were analyzed by TEM. As shown in Figure 3, the cobalt particles were well dispersed on the surface of the CNTs. Some particles penetrated into the channel of the CNTs. This migration may be attributed to the peculiar tubular morphology of the CNTs, which induces capillary forces during the impregnation process. Moreover, acid pretreatment could decrease the hydrophobicity of the CNTs and render the surface more accessible to the aqueous solution of the metal precursor. The particles inside the tubes had sizes of <8 nm, whereas those on the outer surface were as large as 13–25 nm. The CNT channels restricted the growth of the particles inside the tubes.^{26,27} The weak support–metal interaction may be another reason for the larger particles outside the tubes, as cobalt metal easily agglomerates during the calcination and reduction process. The average particle sizes calculated by TEM were

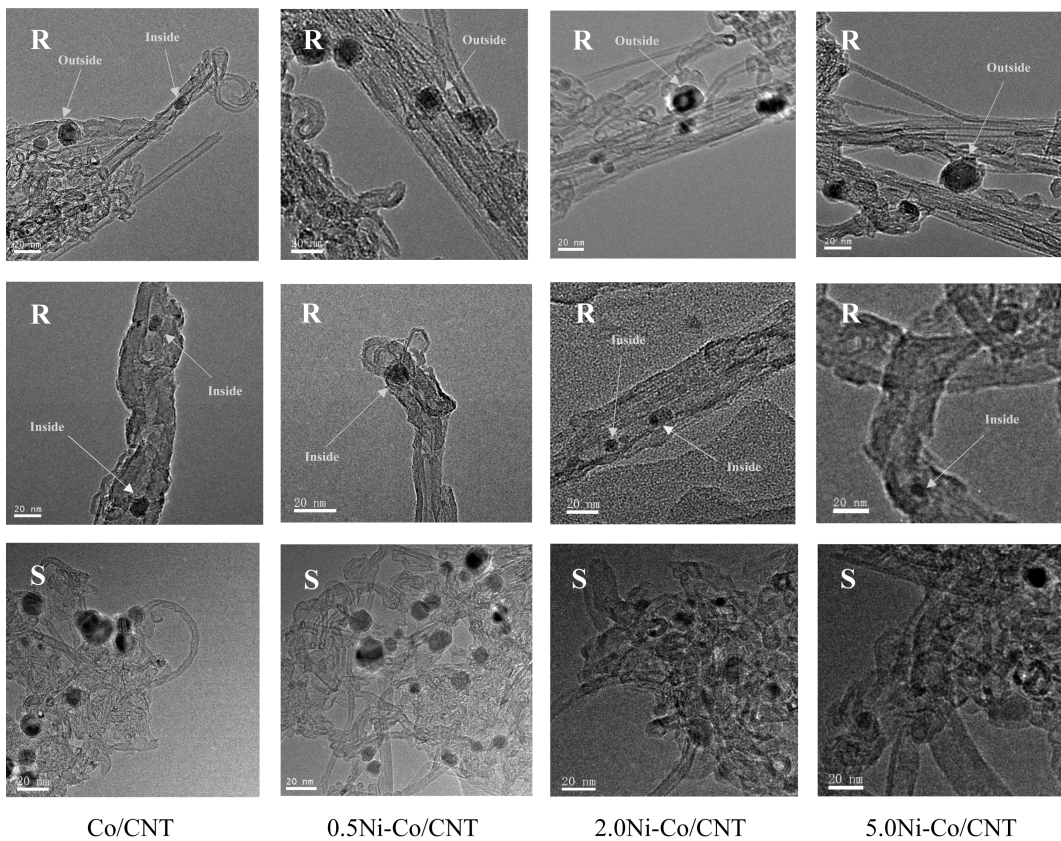


Figure 3. TEM images of the reduced and spent catalysts (R, reduced; S, spent).

10.8, 13.3, 14.5, and 17.8 nm for Co/CNT, 0.5Ni-Co/CNT, 2.0Ni-Co/CNT, and 5.0Ni-Co/CNT, respectively (Table 2). These values were in good accordance with the XRD results.

Figure 4 shows the TPR profiles of the fresh CNTs and the prepared catalysts. The occurrence of several reduction peaks

and NiO.²⁸ Park et al.²⁹ studied the reduction of Co/ γ -Al₂O₃ catalysts and found that the first TPR peak temperature of Co₃O₄ to Co varied between 633 and 643 K and that of CoO to Co varied between 873 and 893 K. Thus, the Co-based CNT catalysts were easily reduced compared with Co/ γ -Al₂O₃. This indicates that much weaker interactions between the Co and CNTs occurred.⁵ The degrees of reduction of the catalysts were determined according to the reoxidation of the reduced catalysts (Table 2). Luo et al.³⁰ reported that the addition of Ni to Co-loaded catalysts could reduce the reduction temperature, which might be caused by the synergistic effect of Co and Ni. In the work presented here, the reduction temperature of the Ni-promoted Co/CNT catalysts also shifted to the direction of lower temperatures (Figure 4). The degree of reduction reached the highest value of 74.0% when the amount of Ni was 0.5 wt %. It is proven that the catalysts can be reduced more completely with smaller particle sizes.²² Therefore, the synergistic effect of Ni and Co and the smaller particle size of 0.5Ni-Co/CNT were both responsible for its highest reduction degree. The wider peak at 823 K for pure CNTs might be caused by the methanation of CNTs.³¹

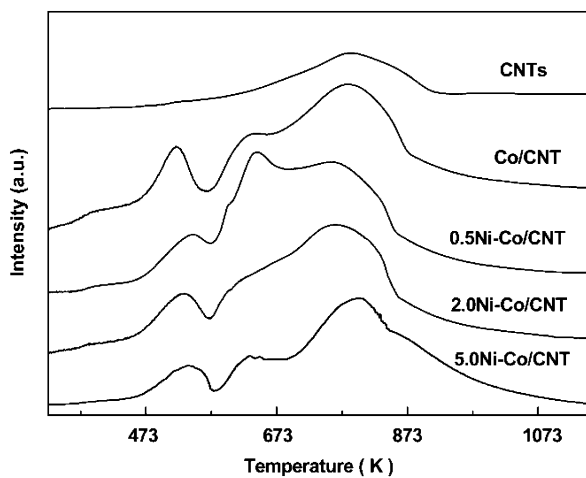


Figure 4. TPR profiles of the prepared catalysts.

indicates the presence of a number of reducible cobalt and nickel species. The first peak at 523–553 K may be attributed to the reduction of Co₃O₄ to CoO. The peak located at 653 K was assigned to the reduction of NiO, which overlapped with the second reduction of CoO to Co. The reduction of the Co-Ni bimetallic catalysts involves two or more overlapping reduction peaks due to the simultaneous reduction of Co₃O₄

3.2. Catalytic Activity and Product Selectivity. The liquid products from the improved FTS process could be divided into the oil phase and aqueous phase. The aqueous phase products mainly consisted of water with small amounts of alcohols, whereas the oil phase contained all of the hydrocarbons, including paraffin, isoparaffin, and small amounts of olefin and cycloparaffin. However, no aromatic hydrocarbons were detected. The main components of the liquid hydrocarbons as determined by GC-MS analysis are listed in Table 3.

Table 3. Main Compositions of the Liquid Hydrocarbons

<i>t</i> _R (min)	compound	relative content (%)	<i>t</i> _R (min)	compound	relative content (%)
1.51	2-methylbutane	1.60	9.03	2-methylundecane	0.60
1.59	3-methylpentane	3.70	9.90	dodecane	3.54
1.71	2-cyclopropylpentane	3.70	10.04	4-methyldodecane	0.55
1.78	heptane	3.84	11.59	tetradecane	3.09
1.92	3-heptene	1.25	12.20	2,5-dimethyldodecane	0.78
2.22	octane	3.62	12.40	2-methyltridecane	0.45
2.32	1,2-dimethylcyclohexane	1.24	13.08	tetradecane	2.35
2.53	4-octene	2.62	13.36	3-methyltetradecane	0.47
2.79	3-ethylheptane	2.39	14.43	pentadecane	2.21
3.20	nonane	3.88	15.23	3-methylpentadecane	0.42
3.51	1,2,3-trimethylcyclohexane	0.85	15.68	hexadecane	1.64
3.84	4-nonene	1.02	16.08	7-methylhexadecane	0.33
4.22	4-methylnonane	3.91	16.85	heptadecane	1.32
5.37	decane	4.17	17.21	7-methylheptadecane	0.28
5.72	1,2-dimethylcyclooctane	0.75	17.97	octadecane	1.04
6.60	2,5-dimethylnonane	1.32	19.03	nonadecane	0.78
7.88	undecane	3.94	20.05	eicosane	0.55

Table 4. Catalytic Performance of Different Catalysts^a

catalyst	<i>X</i> _{CO} (%)	product distribution (C%)				paraffin/olefin (C ₅ –C ₂₀)
		C ₁ –C ₄	C ₅ –C ₂₀	C ₂₁₊	CO ₂	
Co/CNT	90 (90)	24.3 (24.5)	39.0 (39.1)	26.0 (25.8)	10.6 (10.5)	21.1 (20.8)
0.5Ni-Co/CNT	92 (92)	25.2 (25.4)	61.6 (61.5)	6.1 (6.2)	6.8 (6.9)	26.5 (26.6)
2.0Ni-Co/CNT	89 (89)	38.4 (38.3)	53.6 (53.7)	3.4 (3.3)	4.6 (4.7)	23.5 (23.5)
5.0Ni-Co/CNT	81 (81)	46.0 (46.2)	50.1 (49.9)	0.3 (0.1)	3.7 (3.8)	18.7 (18.8)

^aReaction conditions: 533 K, 2 MPa, H₂/CO mole ratio of 2, and GHSV of 1200 h⁻¹. The values in parentheses represent the experimental results after 90 h on stream.

3.2.1. Effect of Ni Promotion. The effect of nickel promotion on the catalytic performance was investigated at a temperature of 533 K, a pressure of 2 MPa, a H₂/CO mole ratio of 2, and a GHSV of 1200 h⁻¹. The catalytic activity and product selectivity are summarized in Table 4. It is observed that the 0.5Ni-Co/CNT catalyst, which had the largest number of Co⁰ active sites (229 μmol/g) (Table 2), showed the highest level of CO conversion.

Previous studies have proven that nickel has a good ability to catalyze the hydrocracking of hydrocarbons.^{11–13} When the nickel promoter was introduced, the heavier hydrocarbons were hydrocracked to lighter ones. In the case presented here, the addition of nickel played an important role in the enrichment of lighter hydrocarbons. As shown in Table 4, the selectivity of 5.0Ni-Co/CNT to gaseous hydrocarbons increased with an increase in Ni content and reached a peak of 46.0%. In contrast, the selectivities of Co/CNT, 0.5Ni-Co/CNT, 2.0Ni-Co/CNT, and 5.0Ni-Co/CNT toward longer-chain products (C₂₁₊) were 26, 6.1, 3.4, and 0.3%, respectively.

Furthermore, it was difficult to avoid the significant increase in the proportion of gaseous hydrocarbons because of the excessive hydrocracking. There is a balance between the carbon-chain growth on the cobalt active sites and the hydrocracking of heavier hydrocarbons on Ni that maximizes the production of liquid hydrocarbons (C₅–C₂₀). Therefore, there is a degree of Ni promotion required for maximizing the selectivity of the catalyst toward liquid hydrocarbons. In this case, the selectivity of 0.5Ni-Co/CNT for liquid hydrocarbons was significantly improved to the highest value (61.6%). A further increase in the level of Ni promotion significantly

increased the level of production of gaseous hydrocarbons and decreased the selectivity for liquid hydrocarbons.

The composition of the liquid hydrocarbon fuel has a great impact on the combustion characteristic and stability. The olefins are especially thermally unstable and may lead to gum formation and deposits in an engine's intake system. Furthermore, toxic dienes may be formed during olefin combustion.³² Therefore, the content of olefins in liquid fuel should be limited. As shown in Table 4, Ni content had an important effect on the content of olefin in the oil phase. The lowest olefin content was obtained over the 0.5Ni-Co/CNT catalyst. Olefin readsorption has a significant influence on the decrease in olefin content in the oil phase. A high surface concentration of hydrogen and the slow diffusive removal of olefin can accelerate the olefin hydrogenation to paraffins and then improve the olefin readsorption.^{33,34} As illustrated in Table 2, the addition of Ni increased the number of Co active sites, especially for 0.5Ni-Co/CNT, which implied an increased number of H atoms adsorbed on the surface of the catalyst. Then olefin hydrogenation was promoted, and then the readsorption of olefin was improved, resulting in a decrease in olefin content in the oil phase. On the other hand, the smallest number of active sites as well as the smallest selectivity of heavier hydrocarbons over 5.0Ni-Co/CNT indicated that there was less H adsorption, which would decrease the possibility of olefin hydrogenation and then increase the selectivity of olefin in the oil phase.

3.2.2. Effect of Operating Conditions. The effect of reaction temperature, H₂/CO mole ratio, pressure, and GHSV on CO conversion and the entire distribution of products were assessed, and the results are listed in Table 5.

Table 5. Effect of Reaction Parameters on Catalytic Performance

catalyst	T (K)	P (MPa)	H ₂ /CO	GHSV (h ⁻¹)	X _{CO} (%)	product distribution (C%)			
						C ₁ –C ₄	C ₅ –C ₂₀	C ₂₁₊	CO ₂
Co/CNT	523	2	2	1200	86.4	22.9	35.6	32.0	9.5
	533	2	2	1200	90.0	24.3	39.0	26.0	10.6
	543	2	2	1200	92.7	40.2	33.0	12.9	13.8
	533	1	2	1200	83.0	26.6	36.7	25.2	11.5
	533	3	2	1200	93.0	27.2	37.8	28.5	6.5
	533	2	1	1200	38.5	22.1	26.5	34.2	17.2
	533	2	4	1200	94.0	47.5	35.8	14.7	2.0
	533	2	2	600	95.0	23.5	38.5	26.6	11.4
	533	2	2	2400	79.5	28.4	38.7	24.0	8.9
0.5Ni-Co/CNT	523	2	2	1200	86.0	24.0	55.3	13.4	7.2
	533	2	2	1200	92.0	25.2	61.6	6.1	6.8
	543	2	2	1200	96.0	36.9	43.3	2.2	17.6
	533	1	2	1200	85.8	26.8	58.3	4.5	10.4
	533	3	2	1200	95.0	28.0	59.8	8.5	3.7
	533	2	1	1200	63.6	23.4	55.5	8.3	12.5
	533	2	4	1200	98.0	50.7	43.0	2.8	3.5
	533	2	2	600	95.5	24.1	59.0	8.4	8.5
	533	2	2	2400	88.0	26.7	60.2	7.5	5.6
2.0Ni-Co/CNT	523	2	2	1200	82.0	35.5	40.5	14.6	9.4
	533	2	2	1200	89.0	38.4	53.6	3.4	4.6
	543	2	2	1200	93.0	45.0	35.6	2.9	16.5
	533	1	2	1200	86.5	39.5	52.0	1.9	6.4
	533	3	2	1200	90.0	38.4	51.6	4.5	5.5
	533	2	1	1200	38.1	30.2	50.5	6.8	12.4
	533	2	4	1200	95.0	70.5	27.5	0.6	1.4
	533	2	2	600	94.0	37.0	49.3	6.3	7.4
	533	2	2	2400	84.4	39.7	51.5	3.2	5.6
5.0Ni-Co/CNT	523	2	2	1200	78.0	41.8	47.5	2.5	8.2
	533	2	2	1200	81.0	46.0	50.1	0.3	3.7
	543	2	2	1200	87.0	47.8	40.4	0	11.8
	533	1	2	1200	79.5	44.0	48.5	0.1	7.4
	533	3	2	1200	86.0	48.0	49.0	0.8	2.3
	533	2	1	1200	47.9	43.8	46.6	2.2	7.4
	533	2	4	1200	94.5	84.0	16.0	0	0
	533	2	2	600	87.0	44.6	49.0	1.5	4.9
	533	2	2	2400	77.0	48.5	48.8	0	2.7

The effect of reaction temperature on product distribution was investigated at 523, 533, and 543 K. The level of CO conversion increased with temperature for each catalyst. Because the mobility of the H atom on the catalyst surface was promoted at higher temperatures, CO conversion was enhanced.³¹ It is shown in Table 5 that a high temperature improved the production of gaseous hydrocarbons, and the same feature was reported by Kwack.³³ The hydrocracking of long-chain hydrocarbons on Ni was improved with an increase in temperature, resulting in more gaseous hydrocarbons and less heavier hydrocarbons. At a proper reaction temperature, 533 K in this case, the carbon chain growing on Co and the cracking on Ni reached a good balance to obtain the highest selectivity of liquid hydrocarbons. The selectivities of liquid hydrocarbons at 533 K, a H₂/CO mole ratio of 2, a P of 2 MPa, and a GHSV of 1200 h⁻¹ were 39, 61.6, 53.6%, and 50.1% for Co/CNT, 0.5Ni-Co/CNT, 2.0Ni-Co/CNT, and 5.0Ni-Co/CNT, respectively.

An increase in pressure would lead to a higher level of CO conversion, which was in accord with previous works.^{33,35} However, the pressure had little effect on product distribution.

Increasing the H₂/CO mole ratio would result in a higher level of CO conversion and higher selectivity of gaseous hydrocarbons for all catalysts, which was in good accordance with the reported results.^{33,36} The H₂/CO ratio of 2 is the optimal value for the highest selectivity of liquid hydrocarbons. Furthermore, 0.5Ni-Co/CNT showed the highest selectivity of liquid hydrocarbons at different H₂/CO mole ratios.

GHSV had a significant influence on CO conversion. The level of CO conversion decreased with an increase in GHSV. However, different GHSV values had little effect on the entire product distribution. Furthermore, 0.5Ni-Co/CNT exhibited a higher selectivity of liquid hydrocarbons than the other catalysts.

Therefore, series of parametric experimental studies showed that the proper amount of Ni loading was important in the production of liquid hydrocarbons. The Co/CNT catalyst with 0.5 wt % Ni loading exhibited the best performance in terms of liquid hydrocarbon production.

3.2.3. Stability of the Catalysts. The stabilities of all the catalysts are shown in Figure 5. The activities of all catalysts underwent an induction period of ~15 h and then reached stable values. Additionally, the catalytic performances of all four

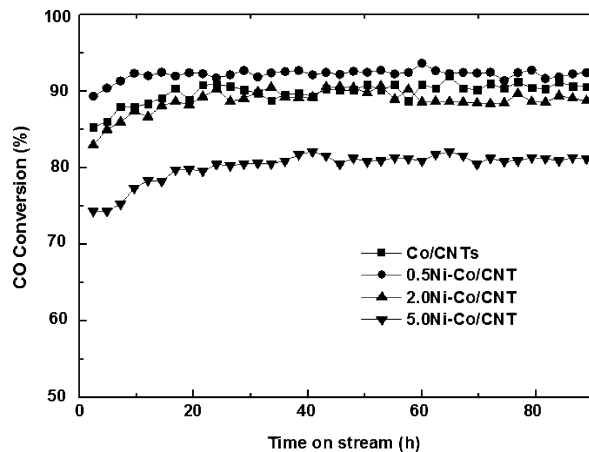


Figure 5. Stability of different catalysts ($T = 533\text{ K}$, $P = 2\text{ MPa}$, H_2/CO mole ratio of 2, and GHSV of 1200 h^{-1}).

catalysts maintained the initial level after 90 h on stream (Table 4). There was no obvious agglomeration of the active components observed (Figure 3). The XRD patterns of the spent catalysts were almost the same as those of the fresh catalysts, which indicated that there was no new phase formed (Figure 2). Therefore, the CNT-supported catalysts performed very well in the FTS reaction with high activity and stability.

4. CONCLUSIONS

A series of Co/CNT catalysts with various degrees of Ni promotion were prepared. Ni promotion had a significant effect on FTS product distribution; it led to an effective decrease in the selectivity for long-chain hydrocarbons and an increase in the selectivity for short-chain hydrocarbons. The reaction temperature and H_2/CO mole ratio had an important effect on product distribution. The 0.5Ni-Co/CNT showed the largest number of active sites ($229\text{ }\mu\text{mol/g}$) and the highest level of CO conversion (92%) at 533 K , 2 MPa , a H_2/CO mole ratio of 2, and a GHSV of 1200 h^{-1} . The selectivity of 0.5Ni-Co/CNT for liquid hydrocarbon fuel ($\text{C}_5\text{--C}_{20}$) reached a highest value of 61.6%. Additionally, all of the cobalt-based CNT catalysts showed excellent stability ($>90\text{ h}$).

■ AUTHOR INFORMATION

Corresponding Author

*Telephone: +86 571 87952801. Fax: +86 571 87951616. E-mail: srwang@zju.edu.cn.

Notes

The authors declare no competing financial interest.

■ ACKNOWLEDGMENTS

We acknowledge financial support from the National Science and Technology Supporting Plan Through Contract 2011BAD22B06, the National Natural Science Foundation of China (51276166), the International Science and Technology Cooperation Program of China (2011DFR60190), the Program for New Century Excellent Talents in University (NCET-10-0741), and the Zhejiang Provincial Natural Science Foundation of China (R1110089).

■ REFERENCES

- (1) Hammache, S.; Goodwin, J. G., Jr.; Oukaci, R. Passivation of a Co-Ru/ γ -Al₂O₃ Fischer-Tropsch catalyst. *Catal. Today* 2002, 71, 361–367.

(2) Xiong, H. f.; Motchelaho, M. A. M.; Moyo, M.; Jewell, L. L.; Coville, N. J. Correlating the preparation and performance of cobalt catalysts supported on carbon nanotubes and carbon spheres in the Fischer-Tropsch synthesis. *J. Catal.* 2011, 278, 26–40.

(3) Tavasoli, A.; Abbaslou, R. M. M.; Trepanier, M.; Dalai, A. K. Fischer-Tropsch synthesis over cobalt catalyst supported on carbon nanotubes in a slurry reactor. *Appl. Catal., A* 2008, 345, 134–142.

(4) Malek Abbaslou, R. M.; Soltan, J.; Dalai, A. K. Iron catalyst supported on carbon nanotubes for Fischer-Tropsch synthesis: Effects of Mo promotion. *Fuel* 2011, 90, 1139–1144.

(5) Zaman, M.; Khodadi, A.; Mortazavi, Y. Fischer-Tropsch synthesis over cobalt dispersed on carbon nanotubes-based supports and activated carbon. *Fuel Process. Technol.* 2009, 90, 1214–1219.

(6) Zhang, H.; Chu, W.; Zou, C. J.; Huang, Z. Y.; Ye, Z. B.; Zhu, L. Promotion effects of platinum and ruthenium on carbon nanotube supported cobalt catalysts for Fischer-Tropsch synthesis. *Catal. Lett.* 2011, 141, 438–444.

(7) Zhu, Y.; Ye, Y. C.; Zhang, S. R.; Leong, M. E.; Tao, F. Synthesis and catalysis of location-specific cobalt nanoparticles supported by multiwall carbon nanotubes for Fischer-Tropsch synthesis. *Langmuir* 2012, 28, 8275–8280.

(8) Knottenbelt, C. Mossgas “gas-to-liquid” diesel fuels: An environmentally friendly option. *Catal. Today* 2002, 71, 437–445.

(9) Ma, W.; Kugler, E. L.; Wright, J.; Dadyburjor, D. B. Mo–Fe catalysts supported on activated carbon for synthesis of liquid fuels by the Fischer-Tropsch process: Effect of Mo addition on reducibility, activity, and hydrocarbon selectivity. *Energy Fuels* 2006, 20, 2299–2307.

(10) Escola, J. M.; Aguado, J.; Serrano, D. P.; Briones, L.; Díaz de Tuesta, J. L.; Calvo, R.; Fernandez, E. Conversion of polyethylene into transportation fuels by the combination of thermal cracking and catalytic hydroreforming over Ni-supported hierarchical beta zeolite. *Energy Fuels* 2012, 26, 3187–3195.

(11) Akhmedov, V. M.; Al-Khowaiter, S. H.; Akhmedov, E.; Sadikhov, A. Low temperature hydrocracking of hydrocarbons on Ni-supported catalysts. *Appl. Catal., A* 1999, 181, 51–61.

(12) Li, X. B.; Wang, S. R.; Cai, Q. J.; Zhu, L. J.; Yin, Q. Q.; Luo, Z. Y. Effects of preparation method on the performance of Ni/Al₂O₃ catalysts for hydrogen production by bio-oil steam reforming. *Appl. Biochem. Biotechnol.* 2012, 168, 10–20.

(13) de Haan, R.; Joorst, G.; Mokoena, E.; Nicolaides, C. P. Non-sulfided nickel supported on silicated alumina as catalyst for the hydrocracking of n-hexadecane and of iron-based Fischer-Tropsch wax. *Appl. Catal., A* 2007, 327, 247–254.

(14) Kang, J. C.; Zhang, S. L.; Zhang, Q. H.; Wang, Y. Ruthenium nanoparticles supported on carbon nanotubes as efficient catalysts for selective conversion of synthesis gas to diesel fuel. *Angew. Chem., Int. Ed.* 2009, 121, 2603–2606.

(15) de la Osa, A. R.; De Lucas, A.; Romero, A.; Valverde, J. L.; Sánchez, P. Influence of the catalytic support on the industrial Fischer-Tropsch synthetic diesel production. *Catal. Today* 2011, 176, 298–302.

(16) Ohtsuka, Y.; Arai, T.; Takasaki, S.; Tsubouchi, N. Fischer-Tropsch synthesis with cobalt catalysts supported on mesoporous silica for efficient production of diesel fuel fraction. *Energy Fuels* 2003, 17, 804–809.

(17) Jacobs, G.; Das, T. K.; Zhang, Y.; Li, J.; Racollet, G.; Davis, B. H. Fischer-Tropsch synthesis: Support, loading, and promoter effects on the reducibility of cobalt catalysts. *Appl. Catal., A* 2002, 233, 263–281.

(18) Bian, G.; Mochizuki, T.; Fujishita, N.; Nomoto, H.; Yamada, M. Activation and catalytic behavior of several Co/SiO₂ catalysts for Fischer-Tropsch synthesis. *Energy Fuels* 2003, 17, 799–803.

(19) González, O.; Pérez, H.; Navarro, P.; Almeida, L. C.; Pacheco, J. G.; Montes, M. Use of different mesostructured materials based on silica as cobalt supports for the Fischer-Tropsch synthesis. *Catal. Today* 2009, 148, 140–147.

(20) Khodakov, A. Y.; Griboval-Constant, A.; Bechara, R.; Zhlobenko, V. L. Pore size effects in Fischer-Tropsch synthesis

over cobalt-supported mesoporous silicas. *J. Catal.* **2002**, *206*, 230–241.

(21) Lv, J.; Ma, X. B.; Bai, S. L.; Huang, C.; Li, Z. H.; Gong, J. L. Hydrogenation of carbon monoxide over cobalt nanoparticles supported on carbon nanotubes. *Int. J. Hydrogen Energy* **2011**, *36*, 8365–8372.

(22) Luisetto, I.; Tuti, S.; Di Bartolomeo, E. Co and Ni supported on CeO₂ as selective bimetallic catalyst for dry reforming of methane. *Int. J. Hydrogen Energy* **2012**, *37*, 15992–15999.

(23) Tsubaki, N.; Sun, S.; Fujimoto, K. Different functions of the noble metals added to cobalt catalysts for Fischer–Tropsch synthesis. *J. Catal.* **2001**, *199*, 236–246.

(24) Li, Y. P.; Wang, T. J.; Wu, C. Z.; Qin, X. X.; Tsubaki, N. Effect of Ru addition to Co/SiO₂/HZSM-5 catalysts on Fischer–Tropsch synthesis of gasoline-range hydrocarbons. *Catal. Commun.* **2009**, *10*, 1868–1874.

(25) Lü, J.; Huang, C. D.; Bai, S. L.; Jiang, Y. H.; Li, Z. H. Thermal decomposition and cobalt species transformation of carbon nanotubes supported cobalt catalyst for Fischer–Tropsch synthesis. *J. Nat. Gas Chem.* **2012**, *21*, 37–42.

(26) Malek Abbaslou, R. M.; Tavasoli, A.; Dalai, A. K. Effect of pre-treatment on physico-chemical properties and stability of carbon nanotubes supported iron Fischer–Tropsch catalysts. *Appl. Catal., A* **2009**, *355*, 33–41.

(27) Trépanier, M.; Tavasoli, A.; Dalai, A. K.; Abatzoglou, N. Co, Ru and K loadings effects on the activity and selectivity of carbon nanotubes supported cobalt catalyst in Fischer–Tropsch synthesis. *Appl. Catal., A* **2009**, *353*, 193–202.

(28) Fazlollahi, F.; Sarkari, M.; Zare, A.; Mirzaei, A. A.; Atashi, H. Development of a kinetic model for Fischer–Tropsch synthesis over Co/Ni/Al₂O₃ catalyst. *J. Ind. Eng. Chem.* **2012**, *18*, 1223–1232.

(29) Park, J.-Y.; Lee, Y.-J.; Karandikar, P. R.; Jun, K.-W.; Bae, J. W.; Ha, K.-S. Ru promoted cobalt catalyst on γ-Al₂O₃ support: Influence of pre-synthesized nanoparticles on Fischer–Tropsch reaction. *J. Mol. Catal. A: Chem.* **2011**, *344*, 153–160.

(30) Luo, N. J.; Kun, O. Y.; Cao, F. H.; Xiao, T. C. Hydrogen generation from liquid reforming of glycerin over Ni–Co bimetallic catalyst. *Biomass Bioenergy* **2012**, *34*, 489–495.

(31) Trépanier, M.; Tavasoli, A.; Dalai, A. K.; Abatzoglou, N. Fischer–Tropsch synthesis over carbon nanotubes supported cobalt catalysts in a fixed bed reactor: Influence of acid treatment. *Fuel Process. Technol.* **2009**, *90*, 367–374.

(32) American Automobile Manufacturers Association, European Automobile Manufacturers Association, Japan Automobile Manufacturers Association. World-wide Fuel Charter, 1998.

(33) Kwack, S. H.; Park, M. J.; Bae, J. W.; Ha, K. S.; Jun, K. W. Development of a kinetic model of the Fischer–Tropsch synthesis reaction with a cobalt-based catalyst. *React. Kinet., Mech. Catal.* **2011**, *104*, 483–502.

(34) Iglesia, E.; Reyes, S. C.; Madon, R. J. Transport-enhanced α-olefin readsorption pathways in Ru-catalyzed hydrocarbon synthesis. *J. Catal.* **1991**, *129*, 238–256.

(35) Yan, Z.; Wang, Z. J.; Bukur, D. B.; Goodman, D. W. Fischer–Tropsch synthesis on a model Co/SiO₂ catalyst. *J. Catal.* **2009**, *268*, 196–200.

(36) Van der Laan, G. P.; Beenackers, A. Kinetics and selectivity of the Fischer–Tropsch synthesis: A literature review. *Catal. Rev.* **1999**, *41*, 255–318.